

# Detecting transition between Abelian and non-Abelian topological orders through symmetric tensor networks

Yu-Hsueh Chen,<sup>1</sup> Ching-Yu Huang,<sup>2,\*</sup> and Ying-Jer Kao<sup>1,†</sup>

<sup>1</sup>*Department of Physics and Center for Theoretical Physics, National Taiwan University, Taipei 10607, Taiwan*

<sup>2</sup>*Department of Applied Physics, Tunghai University, Taichung 40704, Taiwan*

We propose a unified scheme to identify phase transitions out of the  $\mathbb{Z}_2$  Abelian topological order, including the transition to a non-Abelian chiral spin liquid. Using loop gas and string gas states [H.-Y. Lee, R. Kaneko, T. Okubo, N. Kawashima, Phys. Rev. Lett. 123, 087203 (2019)] on the star lattice Kitaev model as an example, we compute the overlap of minimally entangled states through transfer matrices. We demonstrate that, similar to the anyon condensation, continuous deformation of a  $\mathbb{Z}_2$ -injective projected entangled-pair state (PEPS) also allows us to study the transition between Abelian and non-Abelian topological orders. We show that the charge and flux anyons defined in the Abelian phase transmute into the  $\sigma$  anyon in the non-Abelian topological order. Furthermore, we show that both the LG and SG states have infinite correlation length in the non-Abelian regime, consistent with the recent claim that a chiral PEPS has a gapless parent Hamiltonian.

## I. INTRODUCTION

In the past decades, significant efforts have been devoted to understand topologically ordered phases and topological phase transitions. Topological phases [1, 2] cannot be characterized by a local order parameter and can be characterized by properties such as the ground-state degeneracy, and non-trivial quasiparticle statistics [3–7]. Recently, it is realized that these states can be understood through the quantum entanglement, using notions such as topological entanglement entropy [8–10], and entanglement spectrum [11–13]. The latter reveals the edge physics of the topological state, and can be easily computed for the projected entangled-pair states (PEPS) [14], a tensor network that has been successfully represented the ground state wavefunction for systems with both conventional and topological orders. For a symmetry group  $G$ , the  $G$ -injective PEPS [15] forms a natural framework to represent topological ordered systems. It encodes topological properties in the local symmetries on the virtual dimensions. The parent Hamiltonian of a  $G$ -injective PEPS automatically encodes the degenerate ground state subspace and supports anyonic excitations, allowing us to study the topological properties through its entanglement degrees of freedom. However, it is shown that a  $G$ -injective PEPS does not guarantee a topologically ordered phase since the system can be driven into a topologically trivial phase by a physical deformation of the local tensor [16–22]. For example, the phases and phase transitions of the two dimensional (2D) toric code (TC) model with finite string tension, whose ground state is represented by a  $\mathbb{Z}_2$ -injective PEPS [18], can be fully understood within this framework. Similar idea of detecting topological phase transitions has also been generalized to non-Abelian cases recently [23–25].

A new class of  $\mathbb{Z}_2$ -injective ansatz called loop gas (LG) and string gas (SG) is constructed to represent the ground state of the Kitaev models [5] on the honeycomb lattice [26–28]. Surprisingly, when the same ansatz is applied to the Kitaev model

on the star lattice, the entanglement entropy and spectrum suggest that flux anyon in the  $\mathbb{Z}_2$ -topological order become the  $\sigma$  anyon in the non-Abelian chiral spin liquid (CSL) [29]. However, exact results show that the ground state subspace should be three dimensional in the non-Abelian regime [30], inconsistent with the four-fold degenerate ground state structure for the  $\mathbb{Z}_2$ -injective PEPS.

In this paper, we propose to use the overlap of MESs [31] as a unified framework to understand the phase transitions out of a  $\mathbb{Z}_2$  topological order. Using the gauge-symmetry preserved higher-order tensor renormalization group (GSP-HOTRG) algorithm, the overlap can be obtained from the eigenvalue of the corresponding transfer matrix. Our results show that similar to the anyon condensation, the transition from an Abelian to a non-Abelian topologically ordered phase can be understood as both the charge and flux transmute into the  $\sigma$  anyon, resolving the mismatch between the dimension of the ground state subspace for a  $\mathbb{Z}_2$ -injective PEPS and degeneracy of the CSL ground state of the star lattice Kitaev model. We also show that the correlation lengths of LG and SG states diverge in the CSL regime, consistent with the recent claim that the parent Hamiltonian of a chiral PEPS is gapless [32–34].

This paper is organized as follows, In Sec. II, we briefly review the properties of  $\mathbb{Z}_2$ -injective PEPS. In Sec. III, we show the relation between the overlap of MESs and the transfer matrix. In Sec. IV, we revisit the toric code with string tension and demonstrate how to detect anyon condensation transitions using the MES overlap picture. In Sec. V, we apply the method to the Kitaev model on the star lattice and show how to detect the Abelian to non-Abelian topological order transition using MES overlap. We show that the flux and charge anyons transmute into the  $\sigma$  anyon from the full transfer matrix spectrum. We conclude in Sec. VI.

## II. SYMMETRIC PEPS AND ANYONS

A translational invariant PEPS wave function can be written in terms of a local tensor  $A_{\alpha\beta\gamma\delta}^i$  with the physical index  $i$  and

\* cyhuangphy@thu.edu.tw

† yjkao@phys.ntu.edu.tw

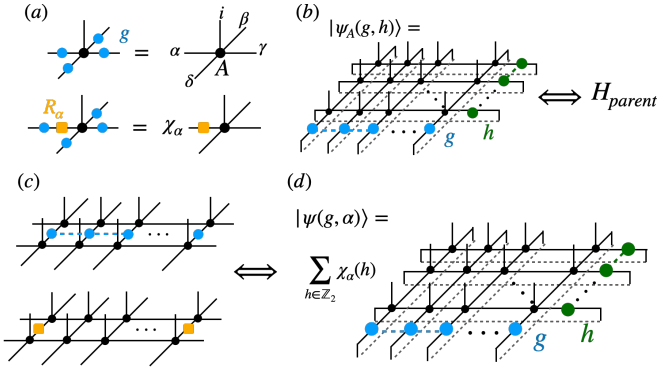


FIG. 1. (a) A  $\mathbb{Z}_2$ -injective PEPS is invariant under  $A(u_g \otimes u_g \otimes u_g^\dagger \otimes u_g^\dagger) = A$ , where  $g \in \{I, Z\}$ . On the other hand, we can find an operator  $R_\alpha$  such that it transforms non-trivially under the group action. (b) For any  $\mathbb{Z}_2$ -injective PEPS  $A$ , we can construct a parent Hamiltonian such that its ground state subspace on the torus is spanned by  $|\psi_A(g, h)\rangle$ ,  $\forall g, h \in \{I, Z\}$ . (c) The anyon excitation can be constructed by either attaching a string of  $u_g$  (flux) or applying  $R_\alpha$  (charge) on the virtual dimension. (d) The MES basis relating to anyon excitations can be constructed through  $|\psi_A(g, \alpha)\rangle = \sum_{h \in \mathbb{Z}_2} \chi_\alpha(h) |\psi_A(g, h)\rangle$ .

virtual indices  $\alpha, \beta, \gamma, \delta$  as

$$|\psi_A\rangle = \sum_{i_1, \dots, i_N} \text{tTr}(A^{i_1} A^{i_2} \dots A^{i_N}) |i_1, i_2, \dots, i_N\rangle, \quad (1)$$

where the tensorial trace is over the virtual indices. A  $\mathbb{Z}_2$ -invariant PEPS [Fig. 1(a)] is represented by a local tensor  $A$  that is invariant under the global  $\mathbb{Z}_2$  symmetry, i.e.,  $A(u_g \otimes u_g \otimes u_g^\dagger \otimes u_g^\dagger) = A$ , where  $u_g$  is a representation of the group  $\mathbb{Z}_2$  with  $g \in \{I, Z\}$ . If  $\mathbb{Z}_2$  is the only symmetry of  $A$ , we say that  $A$  is  $\mathbb{Z}_2$ -injective [15]. For a  $\mathbb{Z}_2$ -injective PEPS, the ground state subspace of the parent Hamiltonian is spanned by the two non-contractible loop operators,  $(u_g^{\otimes L_x}, u_h^{\otimes L_y})$ ,  $\forall g, h \in \{I, Z\}$  acting on the states, which we denote it as  $|\psi_A(g, h)\rangle$  [Fig. 1(b)]. This arises from the fact that the parent Hamiltonian cannot detect these loop operators locally, and we can always use the pull-through condition to deform the non-contractible loop operators. The  $\mathbb{Z}_2$ -injective tensor naturally supports anyonic excitations that cannot be created locally on the systems. For example, a flux excitation can be created by attaching a string of  $u_g$ ,  $g \in \{I, Z\}$  on the virtual bond. A charge excitation can be created by acting an operator  $R_\alpha$  on the virtual bond which transform non-trivially under the group action  $R_\alpha u_g = \chi_\alpha(g) u_g R_\alpha$ , where  $\chi$  is the character and  $\alpha$  designates the irreducible representation of  $\mathbb{Z}_2$  [Fig. 1(c)] [15, 18].

Note that far away from the renormalization group fixed point, the excitation is dispersive and local action of  $u_g$  and  $R_\alpha$  may not correspond to the eigenstates of the parent Hamiltonian. Instead, the excited states should be created by the superposition of local excitations. However, as shown in Ref. [17], these local actions remain crucial to extract anyonic information.

### III. MINIMAL ENTANGLED STATES AND TRANSFER MATRICES

Ground states subspace and the anyonic excitation are closely related, and we can construct a special ground state basis, the minimally entangled states (MESs), to reflect the anyonic excitation of the topological phases. Basically, the MES basis can be obtained by creating a pair of anyons on a torus, wrapping them around a closed non-contractable loop, and finally annihilating them. To be specific, a MES is the eigenstate of the Wilson loop operator with a definite type of anyon excitation; therefore we can construct the MESs in the ground state subspace by  $|\psi_A(g, \alpha)\rangle = \sum_{h \in \mathbb{Z}_2} \chi_\alpha(h) |\psi_A(g, h)\rangle$ , with  $g \in \{I, Z\}$  [Fig. 1(d)]. We then follow the same notation in Ref. [16] to denote  $g = I(Z)$  as  $0(\pi)$ -flux and the parity  $\alpha$ , as even (trivial) and odd (non-trivial). The four MESs  $|I\rangle, |e\rangle, |m\rangle, |\epsilon\rangle$  then correspond to  $|\psi_A(0, e)\rangle, |\psi_A(0, o)\rangle, |\psi_A(\pi, e)\rangle, |\psi_A(\pi, o)\rangle$ , respectively. The overlap of MESs provides the information about the identities of the anyonic excitations and can be obtained from a transfer matrix (TM) [Fig. 2 (a)]. Starting from a local tensor  $A$  representing a  $\mathbb{Z}_2$  topological order, we form a double tensor  $\mathbb{E}$  [Fig. 2 (b)] by contracting the physical indices of  $A$  and its adjoint  $A^*$ ,  $\mathbb{E} \equiv \sum_s (A_{i,j,k,l}^s) \times (A_{i',j',k',l'}^s)^*$ . The corresponding transfer matrix is given by

$$\mathbb{T} \equiv \text{tTr}(\mathbb{E}^1 \mathbb{E}^2 \dots \mathbb{E}^L). \quad (2)$$

The minimally entangled topological sectors corresponding to the quasi-particles can be obtained by inserting the string operator  $Z_g = u_Z^g$ , ( $g = 0, 1$ ) along the cylinder direction and choosing the projector  $P_\alpha$  ( $\alpha = \text{even, odd}$ ) in either the bra or ket. This gives us 16 blocks of transfer matrices. Since each topological sector corresponds to an MES, we can label each block by the overlap of MESs  $\langle a|b\rangle$ , with  $a, b = I, e, m, \epsilon$ . The transfer matrices (Fig. 2 (c)) are defined as

$$\mathbb{T}_{\langle a|b\rangle} = \mathbb{T}_{g', \alpha'}^{g, \alpha} \equiv P_\alpha^{\alpha'} [\text{tTr}(\mathbb{E}^1 \mathbb{E}^2 \dots \mathbb{E}^L Z_g^{g'})] P_\alpha^{\alpha'}. \quad (3)$$

Here  $a = (g, \alpha)$  and  $b = (g', \alpha')$ .  $g$  ( $\alpha$ ) and  $g'$  ( $\alpha'$ ) label the string (parity) operator in the ket and bra layer. The largest eigenvalue  $\lambda_{\langle a|b\rangle}$  of  $\mathbb{T}_{\langle a|b\rangle}$  gives the overlap of the two MESs in the thermodynamic limit.

In the following, we will directly refer the transfer matrix for a given block as  $\langle a|b\rangle$ . The transfer matrices can be divided into four types: (a)  $\alpha = \alpha'$  and  $g = g'$  corresponds to the regular TM computing the norm of the MES,  $\langle a|a\rangle$ , with  $a = I, e, m, \epsilon$  (red color in Fig. 2(c)), (b)  $\alpha \neq \alpha'$  and  $g = g'$  corresponds to the TM measuring the charge difference between the bra and ket (blue), (c)  $\alpha = \alpha'$  and  $g \neq g'$  corresponds to the TM measuring the flux difference between the bra and ket (yellow), (d)  $\alpha \neq \alpha'$  and  $g \neq g'$  corresponds to the TMs measuring the both charge and flux (fermion) difference between the bra and ket (green).

Far away from the renormalization group fixed point, the subleading eigenvalues of the transfer matrix can be interpreted as the excitation energy [17, 35], and the dominant eigenvalues of the transfer matrices measuring the charge (flux) difference can be interpreted as the charge (flux) excitation energy [17]. Similarly, the green blocks in Fig. 2(c) (

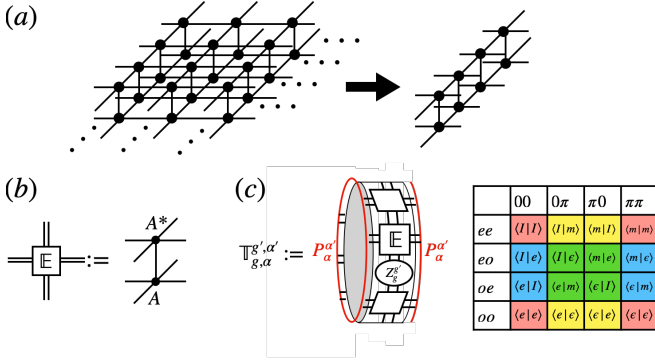


FIG. 2. (a) Overlap of two-dimensional infinite PEPS states can be regarded as a one-dimensional transfer matrix. (b) A double tensor is formed by contracting tensor  $A$  on a lattice site  $a$  with its adjoint tensor  $A^*$  over the physical index. (c) Sixteen blocks of the transfer matrices.

$\alpha \neq \alpha'$  and  $g \neq g'$ ) correspond to the fermionic excitation. This remarkable correspondence makes the relation between MES and anyon more apparent, allowing us to use these 16 transfer matrices to study anyon condensation. As we will discuss in the following section, by tuning the wave function without spoiling the  $\mathbb{Z}_2$ -injectivity, it is possible to drive the system from a topological ordered phase to a topological trivial phase through the condensation of anyons.

It is also possible that an anyon can transmute into another type of anyon. For example, when the  $D(\mathbb{Z}_4)$  quantum double model is continuously deformed to the toric code or the double semion model, some of the anyons distinct in the  $D(\mathbb{Z}_4)$  phase can be identified as the same [18, 19]. Similarly, in the case of the  $\mathbb{Z}_2$ -injective PEPS, we can ask which anyons we can identify as the same.

Since the TM is periodic around the cylinder, we can label the states with the momentum quantum number. Interestingly, it has been shown in Ref. [17] that the momentum quantum number of  $|\epsilon\rangle$  will be shifted by half a spacing, i.e.,  $k = 2\pi(n + \frac{1}{2})/L$ , where  $n = 0, \dots, L-1$  and  $L$  is the circumference of the cylinder. This momentum polarization [36] makes  $|\epsilon\rangle$  impossible to become other MESs. This makes sense in the anyon condensation picture that fermion can never condense (corresponds to  $|\epsilon\rangle \neq |I\rangle$ ), which has been proven in the more general case [18]. Discarding the possibility that  $|\epsilon\rangle$  becomes  $|e\rangle$  or  $|m\rangle$ , we are left with the only choice to identify  $|e\rangle$  and  $|m\rangle$  as the same state. Later we will see that the LG and SG states satisfy this condition.

In order to compute the dominant eigenvalue of each TM block in the thermodynamic limit, we employ the higher-order tensor renormalization group method to merge the sites. To keep the block structure during coarse graining, it is important to carefully preserve the symmetry. Here we develop a GSP-HOTRG method which extends the idea in Ref. [37] to compute the spectrum of the transfer matrices by coarse-graining along the cylinder direction (see App. A for details).

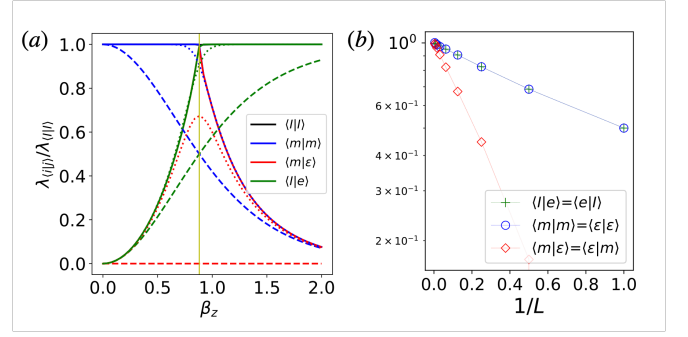


FIG. 3. (a) Dominant eigenvalues of the transfer matrices for TC with  $L = 1$  (dashed lines),  $L = 8$  (dotted lines), and  $L = 256$  (solid lines). (b) Dominant eigenvalues of the transfer matrix for  $\beta_x = 0$  and  $\beta_z = \beta_z^c$  with  $D_{\text{cut}} = 80$ .

#### IV. TORIC CODE WITH FINITE STRING TENSION

Here we revisit the toric code (TC) model with finite string tension, which is the simplest example with the phase transition from a topological order to a topologically trivial phase [16, 17]. We add the string tension by applying the operator  $Q_e(\beta_x, \beta_z) = \exp\left(\frac{\beta_x \sigma_e^x + \beta_z \sigma_e^z}{4}\right)$  to the TC,

$$|\Psi(\beta_x, \beta_z)\rangle = \prod_e Q_e(\beta_x, \beta_z) \times \prod_v \left(1 + \prod_{e \ni v} \sigma_e^x\right) \prod_p \left(1 + \prod_{e \in \partial p} \sigma_e^z\right) |\Omega\rangle, \quad (4)$$

where  $e/p$  labels the the vertex/plaquette, and  $|\Omega\rangle$  indicates the fully polarized spin state  $|\Omega\rangle = \otimes_e |\uparrow\rangle_e$ . For  $\beta_x = 0$  and  $\beta_z \rightarrow \infty$ , the system is driven to the charge condensed (CC) phase. On the other hand, as  $\beta_x \rightarrow \infty$  and  $\beta_z = 0$ , the system is driven to the flux condensed (FC) phase. Therefore, it is expected that by tuning the parameters  $\beta_x, \beta_z$ , phase transitions will occur.

At the  $\mathbb{Z}_2$  topological order (TO) fixed point, the eigenvalues  $\lambda_{\langle a|a\rangle} = 1$ , ( $a = I, e, m, \epsilon$ ), and zero otherwise, indicating these four MESs are orthonormal. At the fixed point of the CC phase,  $\lambda_{\langle I|I\rangle} = \lambda_{\langle I|e\rangle} = \lambda_{\langle e|I\rangle} = \lambda_{\langle e|e\rangle} = 1$ , and zero otherwise, suggesting that sector  $|e\rangle$  is identical to  $|I\rangle$  while  $|m\rangle$  and  $|\epsilon\rangle$  are confined. Similarly, at the fixed point of the FC phase, we have  $\lambda_{\langle I|I\rangle} = \lambda_{\langle I|m\rangle} = \lambda_{\langle m|I\rangle} = \lambda_{\langle m|m\rangle} = 1$ .

Along the  $\beta_x = 0$  axis, there exists a phase transition from the TO to the CC phase as shown in Fig. 3. As we increase  $\beta_z$ , only the regular and charge difference TMs [red and blue blocks in Fig. 2(c)] are non-zero, and there are only four distinct eigenvalues:  $\lambda_{\langle I|I\rangle} = \lambda_{\langle e|e\rangle}$ ,  $\lambda_{\langle m|m\rangle} = \lambda_{\langle \epsilon|\epsilon\rangle}$ ,  $\lambda_{\langle I|e\rangle} = \lambda_{\langle e|I\rangle}$ ,  $\lambda_{\langle m|\epsilon\rangle} = \lambda_{\langle \epsilon|m\rangle}$ . We choose one in each as a representative. The system exhibits phase transition at  $\beta_z = \beta_z^c \approx 0.8814$  [ Fig. 3(a)].

We find  $\lambda_{\langle a|b\rangle}$  does not have significant change for  $L > 256$ ; in the following, we will use  $L = 256$  data to represent the thermodynamic limit. For  $\beta_z < \beta_z^c$ ,  $\lambda_{\langle m|m\rangle} = \lambda_{\langle I|I\rangle} = 1$  and  $\lambda_{\langle I|e\rangle} = \lambda_{\langle m|\epsilon\rangle} < 1$ , which is consistent with Fig. 2(c)

that the blocks in red and blue blocks should be regarded as the same, respectively. For  $\beta_z > \beta_z^c$ ,  $\lambda_{\langle I|e \rangle} = \lambda_{\langle I|I \rangle} = 1$  and  $\lambda_{\langle m|m \rangle} = \lambda_{\langle m|e \rangle} < 1$ . This indicates that the classification in Fig. 2(c) no longer applies; instead, we should identify the blocks in the first (fourth) column as the same. At  $L = 1$  and 8, for  $\beta_z < \beta_z^c$ , while  $\lambda_{\langle I|e \rangle} = \lambda_{\langle m|e \rangle}$  in the thermodynamic limit,  $\lambda_{\langle I|e \rangle}$  is always larger than  $\lambda_{\langle m|e \rangle}$ . This is in fact due to the  $\pi/L$  shift of momentum for  $\epsilon$  as mentioned in Sec. III. In particular, at  $\beta_z = \beta_z^c$ ,  $\lambda_{\langle m|m \rangle}$  and  $\lambda_{\langle I|e \rangle}$  are always the same regardless of the system size, as shown in Fig. 3(b). Therefore, we can accurately identify the critical point by using the crossing of  $\lambda_{\langle m|m \rangle}$  and  $\lambda_{\langle I|e \rangle}$  merely from a single tensor. Note that this is only true for  $\beta_x = 0$ . For  $\beta_x \neq 0$ , if we continuously deform  $\beta_z$ , the crossing point will shift as we keep increasing  $L$ . This arises from the fact that at in this scenario, not only regular and charge difference blocks but the flux and fermion difference blocks are also non-zero. However, even if we fix  $\beta_x$  to other values than 0, after  $L > 4$ , the crossing point is almost fixed, meaning that we can still identify the critical point using very small system sizes.

At  $L = 256$ ,  $\lambda_{\langle I|e \rangle} = \lambda_{\langle m|m \rangle} \rightarrow 1$ . We can interpret  $\lambda_{\langle I|e \rangle} \rightarrow 1$  as  $|e \rangle$  begins to condense and  $\lambda_{\langle m|m \rangle} \rightarrow 1$  as  $|m \rangle$  begins to confine. On the other hand, as mentioned in Sec. III since no other MES can become exactly the same as  $|e \rangle$ , we know that  $\lambda_{\langle m|e \rangle} \rightarrow 1$  indicates a gapless excitation. Similarly, for the TO to FC transition, only the regular and flux difference TMs (red and yellow blocks in Fig. 2(b)) are non-zero. In fact, all the above observations and arguments can be directly adopted to this case once we switch the charge difference to flux difference.

This idea of using the non-vanishing TMs to distinguish phases, surprisingly, can also be extended to the Abelian to non-Abelian TO transition, as we will demonstrate in the next section.

## V. KITAEV MODEL ON THE STAR LATTICE

We extend the ideas developed in the Sec. IV to study the phase transition from an Abelian to a non-Abelian spin TO. We will study the quantum phase transition of the Kitaev model on the star lattice by studying TMs built from the  $\mathbb{Z}_2$ -injective LG and SG states [26–28]. The Hamiltonian is defined as [30]

$$H = -J \sum_{\langle i,j \rangle_\gamma} S_i^\gamma S_j^\gamma - J' \sum_{\langle ij \rangle \in \gamma'} S_i^{\gamma'} S_j^{\gamma'} \quad (5)$$

where  $\langle i, j \rangle_\gamma$  and  $\langle i, j \rangle'_{\gamma'}$  are the pairs on the intratriangle ( $\gamma = x, y, z$ ) and the intertriangle ( $\gamma' = x', y', z'$ ) links connecting site  $i$  and  $j$  as shown in Fig.4(a), respectively. The Hamiltonian can be block diagonalized by the eigenvalues of two types of flux operators defined on the triangle plaquette  $\hat{V}_p = \hat{\sigma}_1^z \hat{\sigma}_2^x \hat{\sigma}_3^y$  and the dodecagon plaquette  $\hat{W}_p = \hat{\sigma}_1^x \hat{\sigma}_2^z \hat{\sigma}_3^y \dots \hat{\sigma}_{12}^y$ , where  $\hat{\sigma}^i, i = x, y, z$  is the Pauli matrix. To gain insights into the model, we consider two extreme limits: the isolated-dimer limit ( $J = 0, J' = 1$ ) and the

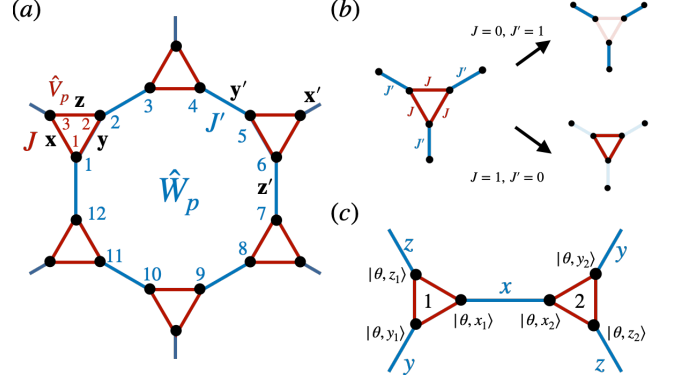


FIG. 4. (a) Star lattice with Kitaev-like interactions. (b) The isolated-dimer and isolated-triangle limits of the Hamiltonian. (c) The initial product state of the LG state.

isolated-triangle limit ( $J = 1, J' = 0$ ) [Fig.4(b)]. The perturbative study in Ref. [38] shows that in the isolated-dimer limit, while the Hamiltonian does not map exactly onto the standard toric code, the ground state is the same as the toric code on the honeycomb lattice. On the other hand, the isolated-triangle limit can be mapped onto the Kitaev honeycomb model at the isotropic point which exhibits a non-Abelian topological order. This suggests that there should exist a phase transition between the two phases. Exact results shows that the model has two distinct gapped phases:  $\mathbb{Z}_2$  topological order when  $J'/J > \sqrt{3}$  and non-Abelian CSL with Ising anyon, when  $J'/J < \sqrt{3}$ . The latter can be distinguished from the former by its three-fold topological degeneracies which can be labeled using MES basis in Ising anyon:  $|I\rangle, |\sigma\rangle, |\epsilon\rangle$ . In both regime, the ground states live in the vortex-free sector  $\{W_p = 1, V_p = 1\}$ .

### A. Loop gas and string gas states

Let us first consider an LG operator:  $\hat{Q}_{\text{LG}} = \text{tTr} \prod_{\alpha} Q_{i_{\alpha} j_{\alpha} k_{\alpha}}^{s s'} |s\rangle \langle s'|$  with the LG tensor defined as

$$Q_{000} = \mathbb{I}, Q_{011} = -iU^x, Q_{101} = -iU^y, Q_{110} = -iU^z. \quad (6)$$

where  $U^\gamma = e^{i\pi S^\gamma}$ ,  $\gamma = x, y, z$  is the  $\pi$ -rotation operator for a given spin (Fig. 5(a)) [28]. One can easily verify that the LG tensor is invariant under the global  $\mathbb{Z}_2$  symmetry on the virtual dimension:  $Q(u_g \otimes u_g \otimes u_g) = Q$  with  $u_g = \mathbb{I}, \sigma^z$ . Therefore, applying  $\hat{Q}_{\text{LG}}$  on any injective PEPS yields a  $\mathbb{Z}_2$ -injective PEPS.  $\hat{Q}_{\text{LG}}$  is a projector to the vortex-free space such that  $\hat{W}_p \hat{Q}_{\text{LG}} = \hat{Q}_{\text{LG}} \hat{W}_p = \hat{Q}_{\text{LG}}$ ,  $\hat{V}_p \hat{Q}_{\text{LG}} = \hat{Q}_{\text{LG}} \hat{V}_p = \hat{Q}_{\text{LG}}$ . Another interesting property of  $\hat{Q}_{\text{LG}}$  is that the creation of flux anyon pair discussed in Sec.II now corresponds to two vortices  $W_p = -1$  at the endpoint of the string  $u_g^{\otimes L}$  [26].

The LG state can then be obtained by applying  $\hat{Q}_{\text{LG}}$  on an initial product state  $|\Psi(\theta)\rangle = \otimes_{\alpha} |\psi_{\alpha}(\theta)\rangle$  where  $\alpha$  is the sites index for a given triangular plaquette and  $|\psi_{\alpha}(\theta)\rangle =$

$|\theta, x_\alpha\rangle|\theta, y_\alpha\rangle|\theta, z_\alpha\rangle$  (Fig. 4(c)). The magnetic state  $|\theta, \gamma_\alpha\rangle$  satisfies

$$\langle\theta, \gamma|\sigma^{\gamma'}|\theta, \gamma\rangle = \delta_{\gamma'\gamma} \cos\theta + (1 - \delta_{\gamma'\gamma}) \frac{\sin\theta}{\sqrt{2}}, \quad (7)$$

where  $\theta$  is a tunable parameter and  $\gamma, \gamma' = x, y, z$ . To simplify the notation, we follow the convention in Ref. [29] to parametrize the Hamiltonian  $H = H(\phi)$  with  $J' = \sin(\phi)$ ,  $J = \cos(\phi)$ . The ground state for a given Hamiltonian  $H(\phi)$  can then be obtained by variationally optimizing the parameter  $\theta$  to find the lowest energy.

To gain more insights, we first consider two limits where the LG state is the exact ground state. In the isolated-dimer limit,  $H(\phi = \pi/2)$ , the ground state degeneracy is exponentially large with the system size, and one of the ground state basis is a product state  $|\Psi\rangle = \otimes_\alpha |\psi_\alpha\rangle$  with  $|\psi\rangle = (|x, +\rangle|y, +\rangle|z, +\rangle)$ , where  $|\gamma, \pm\rangle$  is the eigenvector of  $\sigma^\gamma$  with  $\pm 1$  eigenvalues for  $\gamma = x, y, z$ . This basis is the initial product state for the LG states with  $\theta = 0$  since  $\langle\gamma|\sigma^{\gamma'}|\gamma\rangle = \delta_{\gamma'\gamma}$ , and thus one can identify  $|\gamma, +\rangle = |\theta = 0, \gamma\rangle$ . If we slightly deviate from  $\phi = \pi/2$ , the state is no longer the ground state. However, we expect the ground state of the model to live in the vortex-free sector, and we can apply  $\hat{Q}_{\text{LG}}$  to project it back to the vortex-free space, again giving the LG state at  $\theta = 0$ .

Using the fact that  $Q_{011}, Q_{101}, Q_{110}$  are the  $\pi$ -rotation operator (up to a phase factor) around the  $x, y, z$ -axes, one can derive the resulting state of the LG operator on  $|\theta = 0, \gamma\rangle$  (i.e.,  $|\gamma, +\rangle$ ) as in Fig. 5(b). Now we can combine three different initial states together to form a triangular product state:  $|x, +\rangle|y, +\rangle|z, +\rangle$  (Fig. 5(c)). For a given set of virtual indices, the triangular LG state can be written exactly as the sum of two terms due to the  $\mathbb{Z}_2$ -invariance. Using the relation in Fig. 5(b), one can find that the two terms are exactly the same, as shown in Fig. 5(c). Furthermore, the physical state with different virtual indices, e.g.,  $|y, +\rangle, |y, -\rangle$  and  $|z, +\rangle, |z, -\rangle$  in Fig. 5(c), are orthogonal. This property, combining with the fact the tensor is  $\mathbb{Z}_2$ -invariant, guarantees that the LG state with  $\theta = 0$  is  $\mathbb{Z}_2$ -isometric [15]. Interestingly, the  $\mathbb{Z}_2$ -isometry suggest that LG state at  $\theta = 0$  is the RG fixed point of  $\mathbb{Z}_2$  topological order. This is consistent with the fact that in the isolated-dimer limit, the ground state is the same as the that for the TC on the honeycomb lattice [38]. Note that since SG states is an extension for LG states, it is also  $\mathbb{Z}_2$ -isometric at  $\phi = \pi/2$ . The property of  $\mathbb{Z}_2$ -isometry allows us to view the toric code with string tension (discussed in Sec. IV) and LG, SG with different parameters on the same footing.

On the other hand, in the isolated-triangle limit,  $H(\phi = 0)$ , the LG state is the exact ground state [29, 38]. However, for  $0 < \phi < \pi$ , the energy of the optimized LG state is higher than the exact value [29, 30]. Therefore, instead of using the optimized LG state for a specific Hamiltonian  $H(\phi)$ , in the following we tune the parameter  $\theta$  in the LG state to study its property.

Similarly, for the SG state, we introduce the dimer gas (DG) operator  $\hat{R}_{\text{DG}}(\alpha, \beta) = \text{tTr} \prod_\gamma R_{i_\gamma j_\gamma k_\gamma}^{ss'}(\alpha, \beta) |s\rangle\langle s'|$  with a DG tensor

$$R_{ijk}^{ss'}(\alpha, \beta) = \zeta_{ijk}(\alpha, \beta) [(\sigma^x)^i (\sigma^y)^j (\sigma^z)^k]_{ss'}. \quad (8)$$

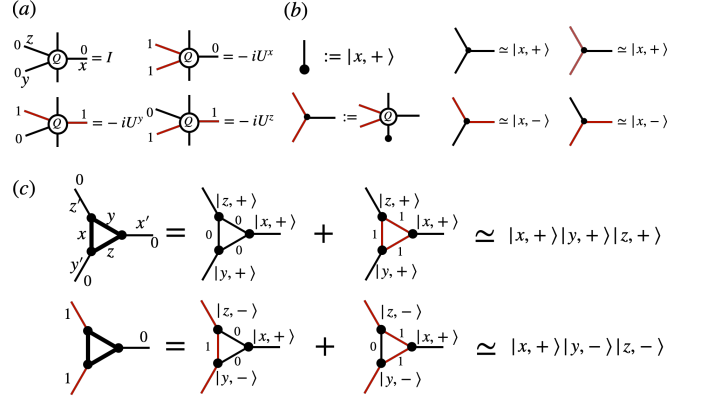


FIG. 5. (a) Non-zero elements of the LG tensor. Here we denote the virtual index 0(1) as black(red) leg. (b) The resulting states (up to a phase factor) of LG operators acting on  $|x, +\rangle$  for a given set of virtual indices. Similar expression can be derived for the initial states  $|y(z), +\rangle$ . (c) The resulting states (up to a phase factor) of LG operators acting on  $|\psi\rangle = |x, +\rangle|y, +\rangle|z, +\rangle$  for a given set of virtual indices. Here we use the thick lines to denote that the virtual legs are contracted.

where

$$\zeta_{ijk}(\alpha, \beta) = \begin{cases} \cos\beta & \text{if } i + j + k = 0 \\ \sin\alpha & \text{if } i + j + k = 1 \end{cases}. \quad (9)$$

The SG state can be constructed as  $|\psi_{\text{SG}}(\alpha, \beta)\rangle = \hat{Q}_{\text{LG}} \hat{R}_{\text{DG}}(\alpha, \beta) |\psi(\theta = \tan^{-1} \sqrt{2})\rangle$  [29]. Since the SG state yields quite accurate ground state energy for the star-lattice Kitaev model, instead of considering the SG state as a two-parameter family of  $\mathbb{Z}_2$ -injective tensor, we label them using the Hamiltonian parameter  $\phi$  instead.

## B. Overlap of minimally entangled states

In the following, we study the topological properties of the LG and SG states by computing the overlap of MESSs, which corresponds to the dominant eigenvalues of the TM blocks,  $\lambda_{\langle a|b\rangle}$ .

As we continuously change the parameter for both the LG and SG states, we find that only the regular and the TMs measuring the fermion difference (red and green blocks in Fig. 2(c)) are non-zero, and there are only four distinct eigenvalues,  $\lambda_{\langle I|I\rangle} = \lambda_{\langle e|e\rangle}$ ,  $\lambda_{\langle m|m\rangle} = \lambda_{\langle e|e\rangle}$ ,  $\lambda_{\langle m|e\rangle} = \lambda_{\langle e|m\rangle}$ , and  $\lambda_{\langle I|e\rangle} = \lambda_{\langle e|I\rangle}$ , while others are zero. Therefore, in each category we choose one as the representative. Note that since  $\lambda_{\langle I|I\rangle}$  is always the largest, we normalize it to 1.

Figure 6 shows the overlaps of the LG states for  $L = 1, 8$ , and 256. For  $L = 1, 8$ , we can see that as  $\theta$  increase from 0 to  $\theta_c = \cos^{-1}(2 - \sqrt{3})$ ,  $\lambda_{\langle m|m\rangle}$  gradually decrease and  $\lambda_{\langle m|e\rangle}$  gradually increase. At  $\theta = \theta_c$ , these two eigenvalues are exactly the same, meaning that we have reached the transition point.

However, if we keep increasing  $\theta$ , the  $\lambda_{\langle m|m\rangle}$  and  $\lambda_{\langle m|e\rangle}$  do not cross. Unlike the level crossing for the charge or

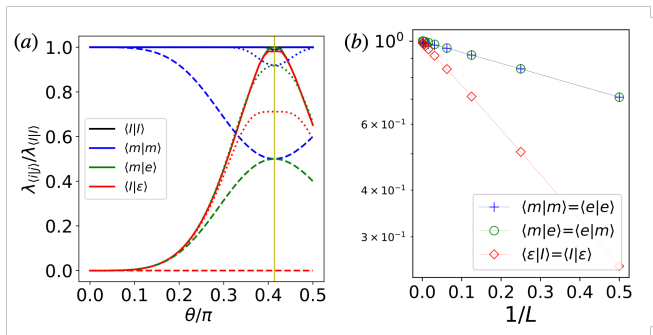


FIG. 6. (a) Dominant eigenvalues of the transfer matrix for LG states with  $L = 1$  (dashed lines),  $L = 8$  (dotted lines), and  $L = 256$  (solid lines). (b) Dominant eigenvalues of the transfer matrix for  $\theta = \theta_c$  with  $D_{\text{cut}} = 80$ .

flux condensation transition in the toric code with string tension (see Sec. IV), here the dominant eigenvalues for the TM blocks only touch, indicating that  $\theta < \theta_c$  and  $\theta > \theta_c$  are in the same phase. At system size  $L = 256$ , we find that  $\lambda_{\langle m|e \rangle} = \lambda_{\langle I|\epsilon \rangle} < 1$  for  $\theta \neq \theta_c$ . This means that  $\langle m|e \rangle$  and  $\langle I|\epsilon \rangle$  should be regarded as the same excitation, and we group them with the same (green) color in Fig. 2(c). Therefore, all the LG states live in the topologically ordered phase, except at  $\theta = \theta_c$ .

At the transition point  $\theta = \theta_c$ , all  $\lambda$ 's approach 1 as the size increases. Similar to the transition points studied in Sec. IV,  $\lambda_{\langle I|\epsilon \rangle} \rightarrow 1$  indicates a gapless excitation; however, we can interpret  $\lambda_{\langle m|e \rangle} \rightarrow 1$  as  $|e \rangle$  and  $|m \rangle$  become the same state. In addition, the spectrum of  $\langle m|\epsilon \rangle$  shows no matter how large the system size is, it will always have two degenerate fixed point; on the other hand,  $\langle m|m \rangle$  and  $\langle \epsilon|\epsilon \rangle$  have a unique fixed point. This means that  $|m \rangle$  can never be identified with  $|\epsilon \rangle$ . We find that  $\lambda_{\langle m|e \rangle}$  is always equal to  $\lambda_{\langle m|m \rangle} = \lambda_{\langle \epsilon|\epsilon \rangle}$  regardless of the system size (see Fig. 6(b)). This argument can also be supported by the calculation of topological entropy  $\gamma$ . We find that both  $|e \rangle$  and  $|m \rangle$  can yield exactly the same  $\gamma = 1/2 \times \ln(2)$  at  $\theta = \theta_c$ , while  $|I \rangle$  and  $|\epsilon \rangle$  give  $\gamma = \ln 2$ . Also, by identifying  $|e \rangle$  with  $|m \rangle$ , we can explain the three-fold degeneracy of the ground state with the correct total quantum dimension  $D = \sqrt{1^2 + 1^2 + (\sqrt{2})^2} = 2$ .

To obtain the SG state for each  $\phi$ , we optimize the free parameters  $\alpha$  and  $\beta$  in Eq. (8) to obtain the variational ground state of Eq. (5). Figure 7 shows the dominant eigenvalues of the transfer matrices constructed from the SG state. Recall that the ground state of the star lattice Kitaev is an Abelian spin liquid at  $\pi/3 < \phi < \pi$ , and non-Abelian at  $0 < \phi < \pi/3$ . For  $\phi = \pi$ , the SG state is  $\mathbb{Z}_2$ -isometric just like the LG state at  $\theta = 0$ . For  $L = 1$ , as  $\phi$  decreases from  $\phi = \pi$  to  $\phi \approx 0.24\pi$ ,  $\lambda_{\langle m|m \rangle}$  gradually decreases and  $\lambda_{\langle m|e \rangle}$  gradually increases. At  $\phi \approx 0.24\pi$ , these two eigenvalues become identical. Different from the transition in toric code charge condensation, if we keep decreasing  $\phi$ , both  $\lambda_{\langle m|m \rangle}$  and  $\lambda_{\langle m|e \rangle}$  increase together. In fact,  $\lambda_{\langle m|e \rangle}$  should never become larger than  $\lambda_{\langle m|m \rangle}$  since the dominant eigenvalues of the regular transfer matrix will always be larger than other blocks

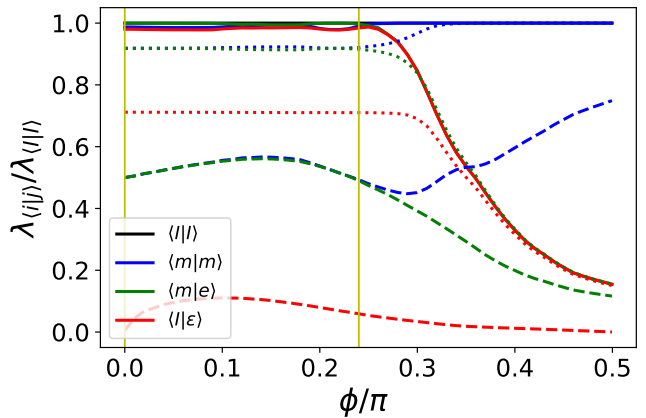


FIG. 7. The dominant eigenvalues of the transfer matrices for the SG states with  $L = 1$  (dashed lines),  $L = 8$  (dotted lines), and  $L = 256$  (solid lines).

for the norm of the states to stay positive. However, the trend for  $\phi < 0.24\pi$  is also different from the LG case. The increase of both  $\lambda_{\langle m|m \rangle}$  and  $\lambda_{\langle m|e \rangle}$  strongly suggest that  $|e \rangle$  becomes  $|m \rangle$  in that regime. This is also consistent with the topological entanglement entropy of  $|m \rangle$  becomes  $1/2 \log(2)$  at  $\phi < 0.24\pi$  [29]. As  $\phi \rightarrow 0$ , both  $\lambda_{\langle m|m \rangle}$  and  $\lambda_{\langle m|e \rangle}$  begin to decrease to the same point as  $\phi \approx 0.24\pi$ , suggesting that we have two transition points at  $\phi = 0$  and  $\phi = 0.24\pi$ .

As we further increase the circumference to  $L = 256$ , all  $\lambda \rightarrow 1$  for  $\phi < 0.24\pi$ . The diverging correlation length suggests that the parent Hamiltonian of the SG states is gapless in this regime. However, as shown in Ref. [33], there might exist other non-frustration-free gapped Hamiltonian, in our case the Kitaev star lattice Hamiltonian, which can also be well approximated by the SG states. This result is also compatible with the no-go theorem [32] that the parent Hamiltonian of a chiral PEPS is gapless.

### C. Transfer Matrix Spectrum

The full spectrum of the transfer matrices labeled by the momentum quantum numbers can be used to support our picture that  $|e \rangle$  and  $|m \rangle$  are identical [17]. In Fig. 8, we observe that not only the dominant eigenvalues match  $\lambda_{\langle \epsilon|\epsilon \rangle} = \lambda_{\langle m|m \rangle} = \lambda_{\langle m|e \rangle}$ , but their full spectra also match. This means that the two MES  $|m \rangle$  and  $|e \rangle$  are exactly the same state. In contrast, while in the thermodynamic limit  $\lambda_{\langle I|I \rangle} = \lambda_{\langle I|\epsilon \rangle}$ , their spectra are always different. This strongly suggests that  $\lambda_{\langle \epsilon|\epsilon \rangle} = \lambda_{\langle m|m \rangle} = \lambda_{\langle m|e \rangle}$  is due to the degeneracy of the state while  $\lambda_{\langle I|I \rangle} = \lambda_{\langle I|\epsilon \rangle}$  is due to the mode softening.

Recall the discussion in Sec. IV, once we drive the  $\mathbb{Z}_2$ -injective wave functions from the TO phase to the CC phase, the original MES basis is no longer the appropriate basis. The  $|e \rangle$  becomes exactly the same as  $|I \rangle$ , and the  $|m \rangle$  is not a physical normalizable state. Similarly, for the LG and SG states in the non-Abelian regime, there exist no charge and flux anyons anymore. Combining with the calculation of entanglement

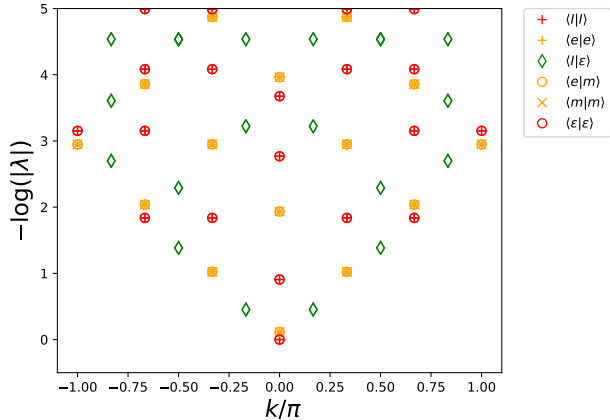


FIG. 8. Transfer matrix spectrum of LG at  $\theta = \theta_c$  with  $L = 6$ .

entropy in Ref. [29], we can regard the charge and flux transmute into  $\sigma$  anyon for  $\phi < 0.24\pi$ . For the honeycomb Kitaev model, the ground state is Abelian when  $|J_x| \geq |J_y| + |J_z|$ , and the extreme limit can be directly mapped to the TC [8]. There, the charge and flux lives in alternating rows of plaquettes. On the other hand, in the non-Abelian phase, all the plaquettes should be regarded equal and the vortex excitation is the  $\sigma$ -anyon. Since the Abelian and non-Abelian limit can be respectively mapped to the TC and the isotropic honeycomb Kitaev model, there exists a critical point where  $|e\rangle$  and  $|m\rangle$  transmute into  $|\sigma\rangle$ . However, the string of  $u_g$  and the charge operator  $R_\alpha$  encode the fusion and braiding rules for the  $\mathbb{Z}_2$  topological order, which can not describe the non-Abelian case. This is the limitation of the  $\mathbb{Z}_2$  classification built in the  $\mathbb{Z}_2$ -injective PEPS. As we show in Sec. VB, the parent Hamiltonian is gapless for  $\phi < 0.24\pi$ , which does not support gapped  $\mathbb{Z}_2$  anyons such as  $|e\rangle$  and  $|m\rangle$ . Within the constraint of the  $\mathbb{Z}_2$ -injective PEPS, the best approximate wave function for a non-Abelian CSL is to make  $|e\rangle$  and  $|m\rangle$  identical. On the other hand, the star lattice Kitaev model is *not* the parent Hamiltonian of the SG states and excitations can be gapped for  $\phi < 0.24\pi$ . This means that the anyonic excitation described by a  $\mathbb{Z}_2$ -injective PEPS may not be the true excitation of the model. Nevertheless, one can create an excitation by the string action  $u_g^{\otimes L} = (\hat{\sigma}^z)^{\otimes L}$ , which will create a vortex pair with  $W_p = -1$  at the endpoints of the string.

## VI. DISCUSSION AND OUTLOOK

Now we have a unified picture to describe the transitions from TO to CC, FC, and non-Abelian phases in terms of the 16 blocks of the TM. The TO to CC transition can be detected when the blue blocks in Fig. 2(c) become distinct. To be more specific, as  $|I\rangle$  and  $|e\rangle$  become the same state,  $|m\rangle$  and  $|\epsilon\rangle$  are confined, and thus  $\langle I|e\rangle$  and  $\langle m|\epsilon\rangle$  are different. Similarly, the emergence of the FC(non-Abelian) phases can be observed as the yellow(green) blocks become distinct. Different from the CC and FC case, the non-Abelian case is not accompanied

with the confinement of other particles. Since the parity even sector of a  $\mathbb{Z}_2$ -invariant tensor is always non-zero, the vacuum state  $|I\rangle$  is always normalizable. In addition, the fact that no other MES can become  $|\epsilon\rangle$ , we conclude that  $\mathbb{Z}_2$ -injective tensors can only detect three types of anyon transitions from identifying the MESs:  $|e\rangle = |I\rangle$ ,  $|m\rangle = |I\rangle$ , or  $|e\rangle = |m\rangle$ . However, there exist other types of topological phase transitions beyond this scheme. For instance, in Ref. [22], it is shown that the self-dual phase transition point of the TC wave function corresponds to the Krammers-Wannier duality of the Ashkin-Teller model, where none of the MESs become identical.

In the current work, we use the  $\mathbb{Z}_2$ -injective PEPS as an example to identify and classify topological phase transitions out the the  $\mathbb{Z}_2$  TO. However, this scheme can be easily generalized to  $G$ -injective and MPO-injective PEPS [39]. The GSP-HOTRG method developed here is a powerful tool to determine whether the system undergoes a phase transition when the PEPS tensor acquires virtual symmetry. The low computation cost of the GSP-HOTRG, same as HOTRG, makes it suitable to perform finite-size scaling analysis, which can be used to extract scaling dimensions at the critical point. Further studies along these directions are worth pursuing.

## ACKNOWLEDGMENTS

This work is partially supported by the Ministry of Science and Technology (MOST) of Taiwan under grants No. 108-2112-M-002-020-MY3, No. 107-2112-M-002-016-MY3, and No. 108-2112-M-029-006-MY3. We thank J. Genzor for collaboration on related work.

## Appendix A: Gauge-Symmetry Preserved HOTRG

We apply the HOTRG coarse-graining scheme to merge tensors along the cylinder direction. Two sites are merged into a single site, generating a rank-6 tensor  $\mathbb{E}' = \sum_{y_2} \mathbb{E}_{x_1, y_1, x_2, y_2} \mathbb{E}_{x'_1, y_2, x'_2, y'_2}$ , where the indices of  $\mathbb{E}$  start on the right and go around clockwise to the top. This can be regarded as a rank-4 tensor by formally grouping the two indices  $(x_1, x'_1)$  on the right to one index, and similarly the two on the left to another. The bond dimension of tensor  $\mathbb{E}'$  along the cylinder direction is the square of the original bond dimension of tensor  $\mathbb{E}$ . Applying an appropriate isometry  $U$  truncates the size of these squared bond dimensions to a fixed number, say,  $D_{\text{cut}}$ , and a truncated tensor  $\tilde{\mathbb{E}}$  can be obtained (Fig. 9).

For  $\mathbb{Z}_2$  topologically ordered phases, we have the  $\mathbb{Z}_2$  gauge symmetry. In our calculation, we only preserve  $\mathbb{Z}_2$  symmetry of the double tensor  $\mathbb{E}$ , i.e., we identify  $(+, +)$ ,  $(-, -)$  as the even sector and  $(+, -)$ ,  $(-, +)$  as the odd sector. Merging two rank-4  $\mathbb{E}$  tensors along the  $y$ -axis, we obtain a new rank-6 tensor  $\mathbb{E}'$  which retains the  $\mathbb{Z}_2$  structure. In order to determine the  $\mathbb{Z}_2$  symmetric isometries,  $U_g (g = 0, 1)$ , we perform eigenvalue decomposition in each block of the  $\mathbb{Z}_2$  block-diagonal

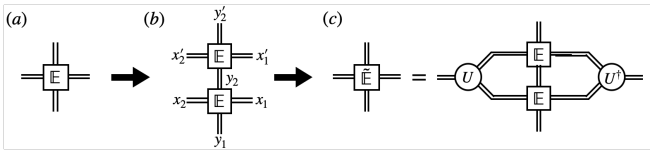


FIG. 9. (a) Start from a one-site double tensor. (b) Merge two double tensors to form a new rank-6 tensor. (c) Apply appropriate isometries  $U$  which truncates the bond dimension

tensor,

$$M_{x_1 x'_3, x_2 x'_3} = \sum_{x_2, x'_2, y_1, y_2} \mathbb{E}'_{x_1, x'_1, y_1, x_2, x'_2, y_1} \mathbb{E}'^*_{x_2, x'_2, y_2, x_3, x'_3, y_2}. \quad (\text{A1})$$

Applying the isometry  $U_g$  in each block generate a truncated tensor  $\mathbb{E}$  which preserve the  $\mathbb{Z}_2$  symmetry. After  $p$  steps of GSP-HOTRG, the final tensor represents a chain of  $2^p$  tensors that preserves the gauge symmetry. The other TMs can be obtained by inserting string operator and choosing different boundary conditions.

- 
- [1] X. G. Wen, Vacuum degeneracy of chiral spin states in compactified space, *Phys. Rev. B* **40**, 7387 (1989).
- [2] X. G. Wen and Q. Niu, Ground-state degeneracy of the fractional quantum hall states in the presence of a random potential and on high-genus riemann surfaces, *Phys. Rev. B* **41**, 9377 (1990).
- [3] X. G. Wen, Topological orders in rigid states, *International Journal of Modern Physics B* **04**, 239 (1990), <https://doi.org/10.1142/S0217979290000139>.
- [4] E. Keski-Vakkuri and X.-G. Wen, The ground state structure and modular transformations of fractional quantum hall states on a torus, *International Journal of Modern Physics B* **07**, 4227 (1993), <https://doi.org/10.1142/S0217979293003644>.
- [5] A. Kitaev, Anyons in an exactly solved model and beyond, *Annals of Physics* **321**, 2 (2006), january Special Issue.
- [6] F. A. Bais and J. C. Romers, The modular S-matrix as order parameter for topological phase transitions, *New Journal of Physics* **14**, 035024 (2012).
- [7] Y. Zhang, T. Grover, A. Turner, M. Oshikawa, and A. Vishwanath, Quasiparticle statistics and braiding from ground-state entanglement, *Phys. Rev. B* **85**, 235151 (2012).
- [8] A. Kitaev and J. Preskill, Topological entanglement entropy, *Phys. Rev. Lett.* **96**, 110404 (2006).
- [9] M. Levin and X.-G. Wen, Detecting topological order in a ground state wave function, *Phys. Rev. Lett.* **96**, 110405 (2006).
- [10] X. Chen, Z.-C. Gu, and X.-G. Wen, Local unitary transformation, long-range quantum entanglement, wave function renormalization, and topological order, *Phys. Rev. B* **82**, 155138 (2010).
- [11] H. Li and F. D. M. Haldane, Entanglement spectrum as a generalization of entanglement entropy: Identification of topological order in non-abelian fractional quantum hall effect states, *Phys. Rev. Lett.* **101**, 010504 (2008).
- [12] F. Pollmann, A. M. Turner, E. Berg, and M. Oshikawa, Entanglement spectrum of a topological phase in one dimension, *Phys. Rev. B* **81**, 064439 (2010).
- [13] A. M. Turner, F. Pollmann, and E. Berg, Topological phases of one-dimensional fermions: An entanglement point of view, *Phys. Rev. B* **83**, 075102 (2011).
- [14] F. Verstraete, V. Murg, and J. Cirac, Matrix product states, projected entangled pair states, and variational renormalization group methods for quantum spin systems, *Advances in Physics* **57**, 143 (2008).
- [15] N. Schuch, I. Cirac, and D. Pérez-García, Peps as ground states: Degeneracy and topology, *Annals of Physics* **325**, 2153 (2010).
- [16] N. Schuch, D. Poilblanc, J. I. Cirac, and D. Pérez-García, Topological order in the projected entangled-pair states formalism: Transfer operator and boundary hamiltonians, *Phys. Rev. Lett.* **111**, 090501 (2013).
- [17] J. Haegeman, V. Zauner, N. Schuch, and F. Verstraete, Shadows of anyons and the entanglement structure of topological phases, *Nature Communications* **6**, 8284 (2015).
- [18] K. Duivenvoorden, M. Iqbal, J. Haegeman, F. Verstraete, and N. Schuch, Entanglement phases as holographic duals of anyon condensates, *Phys. Rev. B* **95**, 235119 (2017).
- [19] M. Iqbal, K. Duivenvoorden, and N. Schuch, Study of anyon condensation and topological phase transitions from a  $F_4$  topological phase using the projected entangled pair states approach, *Phys. Rev. B* **97**, 195124 (2018).
- [20] J. Garre-Rubio, S. Iblisdir, and D. Pérez-García, Symmetry reduction induced by anyon condensation: A tensor network approach, *Phys. Rev. B* **96**, 155123 (2017).
- [21] S. K. Shukla, M. B. Şahinoğlu, F. Pollmann, and X. Chen, Boson condensation and instability in the tensor network representation of string-net states, *Phys. Rev. B* **98**, 125112 (2018).
- [22] G.-Y. Zhu and G.-M. Zhang, Gapless coulomb state emerging from a self-dual topological tensor-network state, *Phys. Rev. Lett.* **122**, 176401 (2019).
- [23] M. Mariën, J. Haegeman, P. Fendley, and F. Verstraete, Condensation-driven phase transitions in perturbed string nets, *Phys. Rev. B* **96**, 155127 (2017).
- [24] A. Schotte, J. Carrasco, B. Vanhecke, L. Vanderstraeten, J. Haegeman, F. Verstraete, and J. Vidal, Tensor-network approach to phase transitions in string-net models, *Phys. Rev. B* **100**, 245125 (2019).
- [25] W.-T. Xu, Q. Zhang, and G.-M. Zhang, Tensor network approach to phase transitions of a non-abelian topological phase, *Phys. Rev. Lett.* **124**, 130603 (2020).
- [26] H.-Y. Lee, R. Kaneko, T. Okubo, and N. Kawashima, Gapless kitaev spin liquid to classical string gas through tensor networks, *Phys. Rev. Lett.* **123**, 087203 (2019).
- [27] H.-Y. Lee, N. Kawashima, and Y. B. Kim, Tensor network wave function of  $s = 1$  kitaev spin liquids, *Phys. Rev. Research* **2**, 033318 (2020).
- [28] H.-Y. Lee, T. Suzuki, Y. B. Kim, and N. Kawashima, Anisotropy as a diagnostic test for distinct tensor network wave-

- functions of integer and half-integer spin kitaev quantum spin liquids (2020), arXiv:2008.10792 [cond-mat.str-el].
- [29] H.-Y. Lee, R. Kaneko, T. Okubo, and N. Kawashima, Abelian and non-abelian chiral spin liquids in a compact tensor network representation, *Phys. Rev. B* **101**, 035140 (2020).
- [30] H. Yao and S. A. Kivelson, Exact chiral spin liquid with non-abelian anyons, *Phys. Rev. Lett.* **99**, 247203 (2007).
- [31] Y. Zhang, T. Grover, A. Turner, M. Oshikawa, and A. Vishwanath, Quasiparticle statistics and braiding from ground-state entanglement, *Phys. Rev. B* **85**, 235151 (2012).
- [32] J. Dubail and N. Read, Tensor network trial states for chiral topological phases in two dimensions and a no-go theorem in any dimension, *Phys. Rev. B* **92**, 205307 (2015).
- [33] T. B. Wahl, H.-H. Tu, N. Schuch, and J. I. Cirac, Projected entangled-pair states can describe chiral topological states, *Phys. Rev. Lett.* **111**, 236805 (2013).
- [34] S. Yang, T. B. Wahl, H.-H. Tu, N. Schuch, and J. I. Cirac, Chiral projected entangled-pair state with topological order, *Phys. Rev. Lett.* **114**, 106803 (2015).
- [35] V. Zauner, D. Draxler, L. Vanderstraeten, M. Degroote, J. Haegeman, M. M. Rams, V. Stojevic, N. Schuch, and F. Verstraete, Transfer matrices and excitations with matrix product states, *New Journal of Physics* **17**, 053002 (2015).
- [36] H.-H. Tu, Y. Zhang, and X.-L. Qi, Momentum polarization: An entanglement measure of topological spin and chiral central charge, *Phys. Rev. B* **88**, 195412 (2013).
- [37] H. He, H. Moradi, and X.-G. Wen, Modular matrices as topological order parameter by a gauge-symmetry-preserved tensor renormalization approach, *Phys. Rev. B* **90**, 205114 (2014).
- [38] S. Dusuel, K. P. Schmidt, J. Vidal, and R. L. Zaffino, Perturbative study of the kitaev model with spontaneous time-reversal symmetry breaking, *Phys. Rev. B* **78**, 125102 (2008).
- [39] N. Bultinck, M. Mariën, D. Williamson, M. Şahinoğlu, J. Haegeman, and F. Verstraete, Anyons and matrix product operator algebras, *Annals of Physics* **378**, 183 (2017).